ICRF-specific W sources: Advances in minimization in ASDEX Upgrade and near-field based extrapolations to ITER with W-wall

Nuclear Materials and Energy 41 (2024) 101742

Contents lists available at ScienceDirect

Nuclear Materials and Energy

journal homepage: www.elsevier.com/locate/nme

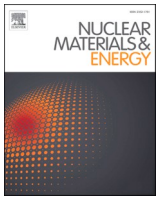

ICRF-specific W sources: Advances in minimization in ASDEX Upgrade and near-field based extrapolations to ITER with W-wall

V. Bobkov [a,*], R. Bilato [a], F. Calarco [b], L. Colas [c], R. Dux [a], G. Grenfell [a], W. Helou [b], D. Milanesio [d], R. Ochoukov [a], F. Paulus [a], Th. Pütterich [a], G. Urbanczyk [a,e], M. Usoltseva [a], the ASDEX Upgrade Team [1]

[a] Max-Planck-Institut für Plasmaphysik, Boltzmannstr. 2, 85748 Garching, Deutschland
[b] ITER Organization, Route de Vinon-sur-Verdon, CS 90 046, 13067 St. Paul Lez Durance Cedex, France
[c] CEA, IRFM, F-13108 Saint-Paul-Lez-Durance, France
[d] Politecnico di Torino, Italy
[e] Institut Jean Lamour UMR 7198 CNRS - Université de Lorraine, 2 allée André Guinier, F-54011 Nancy, France

ARTICLE INFO

Keywords:
ICRF
RF sheath
3-strap
ASDEX Upgrade
Sputtering

ABSTRACT

Experimental data from the 2022 ASDEX Upgrade (AUG) helium (He) campaign reveals that a lower tungsten (W) content can be achieved during operation of the 3-strap antennas with the W-coated limiters. By fine-tuning of electrical feeding of the 3-strap antennas, the core W content was reduced by about a factor of 2 compared to that during operation of the 2-strap antennas with boron coated limiters at the same power and target plasma. This is in contrast to what is observed in deuterium (D) plasmas, where both types of antennas perform similarly in terms of the W release. A higher significance of remote W sources in He than in D is one plausible explanation.

Special AUG experiments in D plasmas, with a density in the SOL reduced to the level relevant for some of the predicted profiles for ITER, show similar characteristics of the near-fields and the sputtering even when the slow wave is propagative. Nevertheless, it is advised for ITER to tailor the SOL profiles by the foreseen local gas injection close to the antenna, to avoid the conditions when the lower hybrid resonance position is approximately aligned with the position the leading edges of the plasma facing components.

Based on near-field calculations for the AUG 3-strap and the ITER ICRF antennas using the HFSS code under the same conditions, the experimentally validated RF-sheath rectified voltages of the AUG 3-strap antenna were scaled to the ITER ICRF antenna. Using conservative assumptions, the estimations of the ICRF-specific W sources for ITER were then made for the D-T case with neon seeding. The extrapolation shows that by carefully choosing the electrical feeding, the increment of the W sputtering rate during ITER ICRF operation at up to 20 MW, can be kept (in the worst case) below 10 % of the total W wall rate without ICRF, as well as below 25 % of the W rate at the outboard wall without ICRF.

1. Introduction

Sputtering of the full-tungsten (W) wall due to the RF sheath effects during operation of the Ion Cyclotron Range of Frequencies (ICRF) antennas has been extensively studied in ASDEX Upgrade (AUG) [1]. These studies and the AUG experimental experience are becoming increasingly important for ITER in view of the re-baselining which aims at operations with the full-W first wall [2,3]. One ICRF antenna is planned for the ITER so-called SRO (Start of Research Operation) phase, with a further increase to 20 MW in the DT-1 (deuterium – tritium) operational phase if its effectiveness in an all-W ITER has been confirmed.

In this work, we report on further studies of the residual W release associated with the near-field–optimized AUG 3-strap ICRF antennas and on the importance of the antenna feeding control. This includes aspects of characterization at very low Scrape-Off-Layer (SOL) density which represents special conditions for AUG, but an operational corner expected for some of the ITER plasmas. After this, we provide conservative estimates of the ICRF-specific W sources for ITER based on a near-

* Corresponding author.
E-mail address: bobkov@ipp.mpg.de (V. Bobkov).
[1] See the author list of "H. Zohm et al, 2024 Nucl. Fusion **64** 112001".

https://doi.org/10.1016/j.nme.2024.101742
Received 23 May 2024; Received in revised form 30 August 2024; Accepted 19 September 2024
Available online 21 September 2024

field scaling of the AUG 3-strap and the ITER ICRF antennas with optimized feeding.

2. AUG helium plasmas

It was shown in the previous AUG studies of the ICRF-specific W sources and optimization of the ICRF antennas [4,5], that the optimized 3-strap antennas with the W-coated limiters compare well to the 2-strap antennas with the boron (B) coated limiters. This was achieved using the principle of cancellation of the RF image currents on Plasma Facing Components (PFCs). For the antennas with 3 or more toroidally distributed straps in dipole phasing, the RF image current contributions by the straps closest to the PFCs ("outer" straps) can be nearly cancelled by the out-of-phase contributions from the centre of the antenna ("central" straps). After the successful application in AUG, this principle has been tested in Alcator C-Mod [6] and in JET [7]. In AUG, deuterium (D) plasmas with hydrogen (H) minority heating scenario, the residual W contamination when using the W-coated 3-strap antennas (*a2* and *a4* in Fig. 1) approximately equals to that of the B-coated 2-strap antennas (*a1* and *a3* in Fig. 1). This indicates that the sum of contributions of the local (antenna limiters) and of the remote W sources attributed to the ICRF heating by the 3-strap antennas is approximately equal to the contribution of the remote W sources by the 2-strap antennas in D plasmas. By remote W sources we define all the W sources which are not located at the antenna limiters. Helium (He) plasmas present the most challenging environment for ICRF operation with high-Z walls, because the majority species (mostly double-charged ions He^{2+}) is able to sputter W directly already at low accelerating rectified RF sheath voltages (~few tens of volts, depending on T_e in the SOL). In the He plasmas with H minority heating, early indications were observed that the W-coated 3-strap antenna can produce marginally lower W source at the same RF power [5].

Fig. 2 summarizes the data on ICRF-specific increments of W concentration (Δc_W, Fig. 2(a)) measured by VUV spectroscopy at $T_e \approx 1.5$ keV and of the W limiter source (Δc_W, Fig. 2(b)) measured by visible spectroscopy (see Fig. 1), from the more recent (2022) experiments in He H-mode plasmas at −2.5 T with 4 MW of ECRH and constant

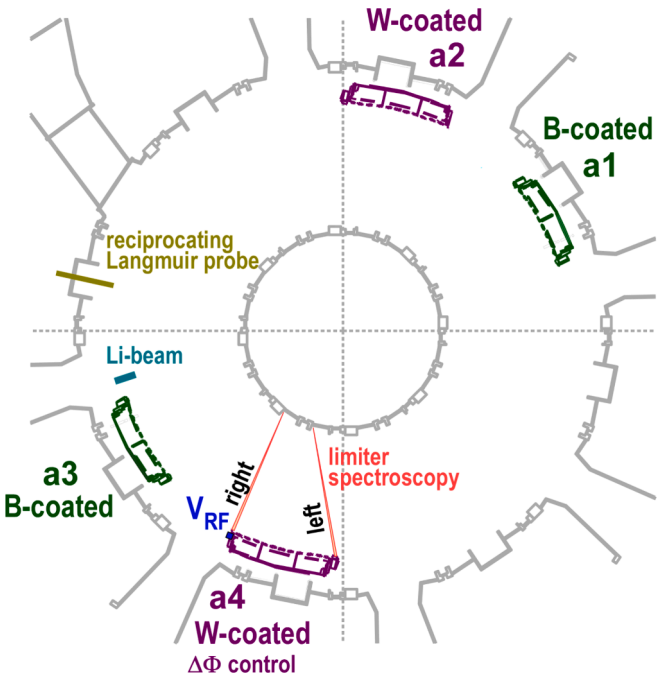

Fig. 1. Setup of AUG ICRF antennas and measurements. *a1/a3* (and independently, *a2/a4*) constitute an operational pair connected within the single RF network.

P_{ICRF}=1 MW at 36.5 MHz. Fine scans were implemented around the optimum antenna feeding in terms of the power fraction of the central strap to the total power P_{cen}/P_{tot} and the phasing deviation from the *dipole* ΔΦ. The definition and control of the *dipole* phasing in experiment has previously been made within 10° accuracy, usually sufficient for D. However, Fig. 2 shows that in He, 10° can make a significant difference and that it is critical to control the feeding of the antenna more precisely. In these He cases, a special attention was given to phase steering using the new control system [8]. In AUG, the phase is controlled for one 3-strap antenna only (*a4* in this case). For the other antenna (*a2*), it is defined by the symmetry and tuning of the RF feeding network. Every point from Fig. 2 is an average over 250 ms at the end of the 400 ms long time intervals with constant P_{cen}/P_{tot} and phasing. The plasma density close to the antenna limiters was approximately constant.

Fig. 2(a) shows that, with the precise phase control, Δc_W for the W-coated 3-strap antennas with P_{cen}/P_{tot} = 0.6 and ΔΦ=0° can be kept about a factor of 2 lower than that for the B-coated 2-strap antennas. This is the first example showing that the W-coated 3-strap antennas clearly outperform the B-coated 2-strap antennas in terms of W release. However, in contrast to typical situations in D-plasmas (see e.g. [4]), the reasons for this are not directly evidenced in the measurements of the W source at the antenna limiters (Fig. 2(b)). The local W sources at the limiters, at least those measured on the existing lines of sight of the spectroscopic measurements (see Fig. 1) which cover predominantly the upper half of *a4*, do not fully correspond to the tendencies of Δc_W. In particular, in the case with ΔΦ=+10° the local W source is increased, but not with ΔΦ=-20°, although both cases are characterized by increased Δc_W. In addition to possible changes of the local W source in the non-observed (lower, with vertical coordinate $z < -0.01$) regions of the antenna limiters, one can invoke non-local W sources as likely contributors to this behaviour. It is however difficult to pinpoint more specifically where these remote sources are located, as the divertor W sources were not measured during these experiments. Δc_W measured at the *a4* limiters when only the 2-strap antennas are powered (shown close to P_{cen}/P_{tot} = 0.5 in Fig. 2(b)) is an example of such a non-local W source. And for most cases in Fig. 2, it is comparable to the local W source at the active 3-strap antenna (when *a4* is powered). In parallel to the propagation of the rectified sheath perturbations along the magnetic field lines connected to powered ICRF antennas (see [5,9] and references therein), also the effects of the non-absorbed power fraction at low [6,10] and high $k_{||}$ [6] can play a role. The latter can lead to the far fields in the SOL and thus also to the remote ICRF-specific W sources. The high sensitivity to the phasing and presumably the higher relative importance of the remote W sources in He is likely caused by the high W sputtering yield by the main species. Furthermore, only the total (thermal and RF rectified) sheath voltages of ~ 50 V are needed for strong W sputtering by the double-charged He ions. Therefore, in He, the W sputtering yield is higher and its dependence on the sheath voltage is sharper compared to the D plasmas, where only the light impurities with relatively low concentrations sputter W.

One can summarize that for ITER, a precise feeding control with the accuracy in phasing much better than 10° is essential. Fortunately, for an antenna with 3 or more toroidal straps, the feeding requirements to minimize the near-field induced local effects and the remote effects due to the propagation of the rectified sheath perturbation along the magnetic field lines approximately coincide with those to minimize the far fields caused by the RF power carried by unfavourable $k_{||}$ (see section 3.1 in [11]).

One nuance for ITER is that in some cases, in contrast to the standard conditions in the existing experiments, plasma density profiles with the density below the Lower Hybrid (LH) density $n_{e,lh}$ in the SOL in front of the PFCs are predicted. The next section aims to study similar conditions experimentally in AUG.

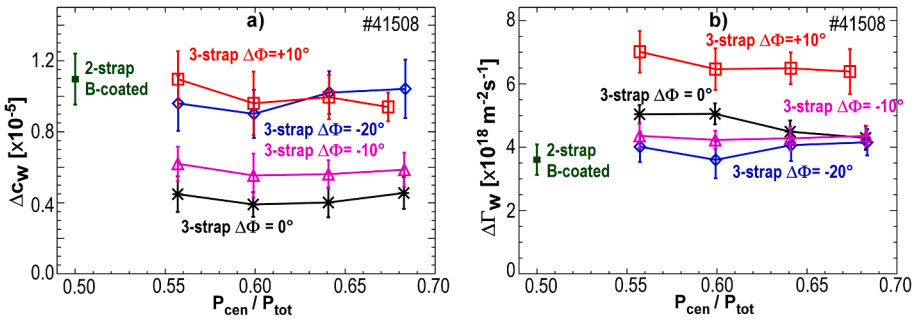

Fig. 2. ICRF-specific increments of: (a) the W concentration at $T_e \approx 1.5$ keV Δc_W and; (b) the W influx spatially averaged over all lines of sight at the *a4* antenna limiters $\Delta\Gamma_W$; as functions of P_{cen}/P_{tot} for various $\Delta\Phi$. Values close to $P_{cen}/P_{tot} = 0.5$ show Δc_W and $\Delta\Gamma_W$ measured when only the 2-strap antennas are powered.

3. AUG low density D SOL

Condition $n_e = n_{e,lh}$ corresponds to the LH resonance and is considered as a qualitative boundary, because the slow wave (SW) can propagate at $n_e < n_{e,lh}$. This is the same wave as used for the LH current drive, but it is confined to low densities for ICRF and it carries the parallel electric field $E_{||}$ known to be the major contributor to the ICRF sheath effects. In the current machines, the SW propagation region is usually narrow in the PFC shadow and on the leading edges of PFCs the SW is evanescent. For ITER, in some configurations the region of propagative SW extends towards the plasma core and covers a finite radial range in front of the PFCs. In AUG, this region can be artificially extended in special, very low-density plasmas with high plasma-wall clearance. This was done in [12] which identified that indeed the SW can propagate in the form of the so-called resonance cones in the low-density SOL in D plasmas and can be tracked. In such AUG scenario, 3-strap antennas were operated at $P_{ICRF} \approx 160$ kW at 36.5 MHz with 0.7 MW of ECRH. The relevant data is shown in Fig. 3.

Three experimental density profiles are shown in Fig. 3(a): cases (1) and (2) with $n_e < n_{e,lh}$ at the antenna limiter and case (3) with $n_e > n_{e,lh}$ at the limiter. The density close to the limiter and up to about 5 cm in front of the limiter was measured using the reciprocating Langmuir probe (yellow-green highlighted region in Fig. 3(a)). Beyond that, the density was measured by the Li-beam (Fig. 1). These diagnostics are located at about the same vertical position $z = 0.3$ m. The local equivalent RF voltage V_{RF} (derived from the RF current as in [5]) at the *a4* limiter and the ICRF-specific increment of W influx Δc_W on the right limiter of *a4* close to z = 0.3 m are shown in Fig. 3(b) and Fig. 3(c) respectively. The use of Δc_W in the context of the near-fields instead of ΔY_W (increment of the sputtering yield) is justified by the effect of variation of light impurity content on ΔY_W being partially compensated by the effect of impinging particle density on Δc_W. Thus Δc_W acts as a better proxy of the near-field effect when comparing density profiles. The quantities are normalized to $\sqrt{P_{ICRF}}$ to compensate for variations of the RF power in the first (linear) approximation. Power balance scans in the dipole phasing were performed. Instead of P_{cen}/P_{tot}, voltage ratio V_{cen}/V_{out} (ratio of the maximum voltage in the transmission line of the central strap to that of the outer straps) is used on the horizontal axis with a regular grid in Fig. 3(b) and Fig. 3(c). This is because at low ICRF coupling, a large discrepancy exists between the RF power measured close to the antennas in the unmatched lines and the RF power in the matched lines. In AUG, the latter is usually assumed as a proxy for the former (which is unavailable), but here this assumption would be too imprecise.

Fig. 3(a) and 3(b) show that there is no qualitative difference between all the three density profile cases, and the optimal feeding weakly depends on density. All of the cases exhibit a similar minimum, independently whether $n_e < n_{e,lh}$ at the limiter (profiles (1) and (2)) or not (profile (3)). The higher V_{RF} and higher Δc_W at lower densities are not new observations and are expected from the previous studies. The explanations involve effects due to lower plasma RF conductivity and higher light impurity content and plasma temperature at lower densities

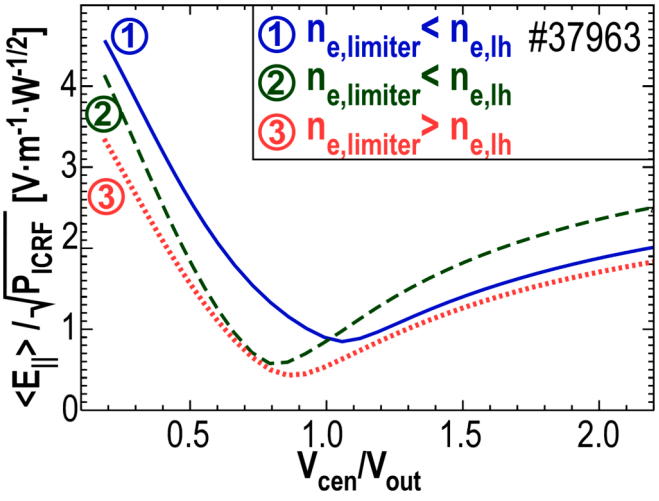

Fig. 4. Near-field TOPICA calculations corresponding to the local observations and density profiles from Fig. 3.

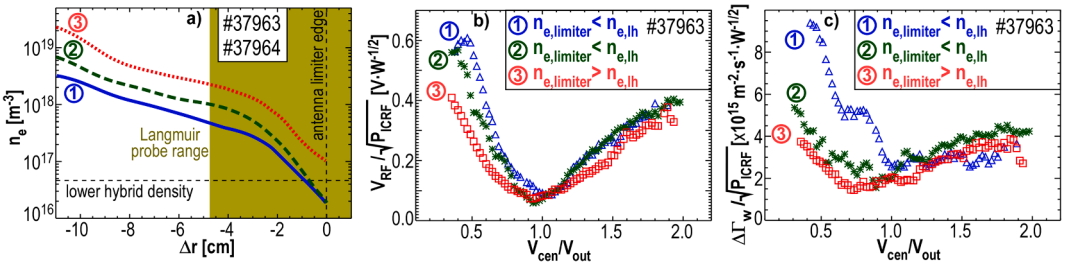

Fig. 3. a) Density profiles from Langmuir probes and Li-beam measurements at $z \approx 0.3$, as a function of distance to the limiter; for profiles 1 and 2: $n_e < n_{e,lh}$ at the limiter; b) V_{RF} on the right *a4* limiter (as seen from plasma, see Fig. 1) at $z \approx 0.3$; c) $\Delta\Gamma_W$ on the right *a4* limiter at $z \approx 0.3$. V_{RF} and $\Delta\Gamma_W$ are normalized to $\sqrt{P_{ICRF}}$.

(see e.g. [1,9] and references therein). Furthermore, as Fig. 4 shows, the behaviour is well consistent with normalized local $<E_{||}>$ calculated by TOPICA [13] (also acting as a proxy for the sheath voltage) for the three density profiles without considering the SW propagation.

Thus, there is so far no indication of a strong impact of the propagating SW on the behaviour of the local RF properties and sputtering at the ICRF antenna PFCs. This result is insofar unsurprising as the previous experimental studies, in particular of the ICRF-specific heat loads, (see e.g. [14]) do not report noticeably increased heat loads in the lower density regions of the antenna PFCs. Such increased heat loads could be expected if the propagating SW increases significantly the rectified RF sheath voltages, because the heat loads should not saturate at high ion energies. The opposite trend is observed: the regions with the highest densities are characterized by the highest heat loads. Still, with the LH resonance in front of the PFCs, the propagating SW remains a potential cause of the parasitic power absorption in the SOL [10] and of the far-fields. It is also advisable to avoid alignment of the LH resonance with the leading edges of the PFCs, i.e. $n_e \approx n_{e,lh}$ at the limiter. Such alignment is difficult to achieve in experiments, but can in theory lead to focusing of the RF power carried by the resonance cones on the PFC leading edges. In ITER this can be avoided using the local gas injection [15] to tailor the density profiles in front of the antenna PFCs, presumably at low gas puff rates.

The fact that there is no indication pointing on the propagative SW (at $n_e < n_{e,lh}$) as an important contributor to the RF fields and the W sputtering at antenna PFCs and the fact that the optimal antenna feeding weakly depends on density are encouraging results for ITER. This allows to further use the existing guidelines [1] to reduce the sputtering, and to conduct a simplified scaling of the sheath voltages based on the relative comparisons of the antennas in terms of the near-fields, including the LH density range.

4. Extrapolations to ITER

The AUG 3-strap antenna image current cancellation principle can be successfully applied to the current ITER ICRF antenna design with 4 toroidal columns of straps. In order to put the performance of the ITER antenna with optimized antenna feeding in terms of W sources into perspective, we compare at first the $E_{||}$ near-fields at PFCs for both the AUG 3-strap antenna (Fig. 5(a)) and for the ITER antenna (Fig. 5(b)) using HFSS [16] models with the same lossy dielectric (sea water) loading and with the same PFCs. Then, using the near-field comparison and the validated AUG experimental results, as well as the known dependencies of the W sputtering yield on impinging species, we scale the W sources to the specific conditions relevant for ITER. A more detailed description is available as ITER report [17]. A more sophisticated approach in estimating the ICRF-specific W sources is described in [18].

Fig. 6(a) shows the comparison of the average parallel field $<E_{||}>$ calculated in the regions illustrated in Fig. 5 for various antennas and feedings, for the distance between the antenna and the loading (see Fig. 5) $d = 8$ cm. Fig. 6(b) presents results of extended calculations with various values of d. For the ITER antenna, toroidal phasings (0; π; π; 0) and (0; π; 0; π) are considered with phasings between the two poloidal antenna halves (0; π) and (0; −π/2). For these feedings, $<E_{||}>$ is compared to $<E_{||}>$ of the AUG 3-strap antenna with optimized feeding ((0;π;0) with $P_{cen}/P_{tot} \approx 0.6$) in Fig. 6(a) and is normalized to the latter in Fig. 6(b). The comparison is on the conservative side for the ITER antenna, as it favours reduction of the 3-strap antenna image currents which decay more efficiently on the larger conductive area around the antenna.

The ITER antenna feeding of (0; π; π; 0)(0; π) is conceptually the closest to the 3-strap antenna and has very similar $<E_{||}>$. From all the ITER antenna feeding phasings, only (0; π; π; 0)(0; −π/2) "balanced" with uniform power distribution is not optimized for lowest $<E_{||}>$. The dashed curve in Fig. 6(b) shows that in this case, $<E_{||}>$ can be reduced by increasing the phase by 5°, confirming that the precise phase control is crucial, as discussed in section 2. For the feedings with optimized $<E_{||}>$, ITER antenna compares well with the AUG 3-strap antenna: all (0; π; 0; π) "tapered" ($P_{cen}/P_{tot} \approx 0.8$) cases show noticeably lower $<E_{||}>$ than that for the 3-strap antenna.

Approximated ranges of the sheath accelerating voltage and effective sputtering yield Y_W observed in AUG experiments, which are backed up by simulations of the 2-strap and the 3-strap antenna (see [1,4,5,19,20] and references therein), are summarized in Fig. 7. Y_W is calculated based on the examples with the light impurity contents from [19], one for the case without boronizations (orange), one for the case with regular boronizations (black). Curves for single ionized and for multi- ionized (based on average charge states estimated for coronal equilibrium) including contributions from W self-sputtering (simplified model) are shown. The upper estimate for the 3-strap antenna induced sheath voltage of about 90 V with 1 MW of power is taken and the sheath voltage is scaled to the ITER antenna using the near-field results presented in Fig. 6, but excluding the (0; π; π; 0) "balanced" feeding. The voltages are kept constant throughout the whole density range, providing conservative estimates.

The ICRF-specific W sputtering in ITER is estimated for the "worst case" for the W sources at ITER: D-T plasma with 2 % of neon (Ne) with charge state distribution 28 %Ne^{10+}+22 %Ne^{9+}+34 %Ne^{8+}+16 %Ne^{7+} as the dominant light impurity species during seeding in the D-T mixture, provided by the ITER Organization (IO) as input to [17]. The estimates are made under the assumptions of constant light impurity content and constant $T_e = 20$ eV with $T_i = 2 \cdot T_e$. This naturally leads to the W sputtering flux and W sputtering rate being as a quantity proportional to density n_{e0} at the edge of the antenna PFCs. As could be followed from the section 3 discussion, such assumptions do no precisely describe typical experimental situations during density scans. On the other hand, we use the assumptions to provide conservative (upper limit) W source estimates.

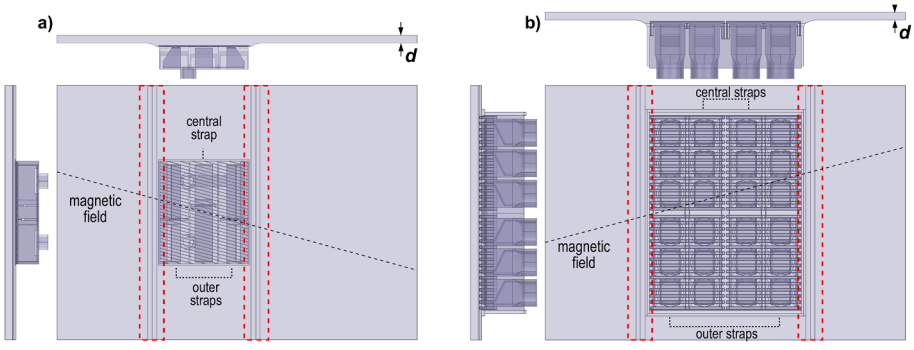

Fig. 5. Antenna models for near-field comparison: a) AUG; b) ITER. Dashed red rectangles show areas of $E_{||}$ assessment. (For interpretation of the references to colour in this figure legend, the reader is referred to the web version of this article.)

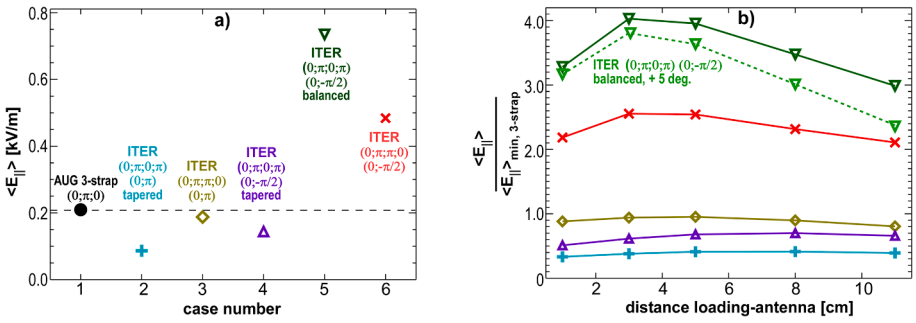

Fig. 6. Near field comparison. a) $< E_{||} >$ for $d = 8$ cm; b) normalized to $< E_{||} >$ the 3-strap antenna as a function of d.

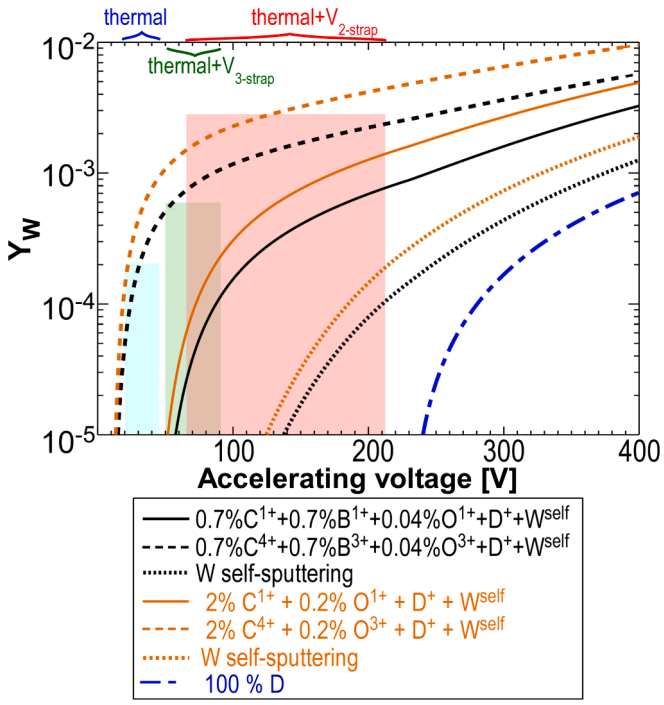

Fig. 7. Summary of AUG observations and approximate regions covered by experiments. Orange: light impurities w/o boronizations, black: with bornozations [16]. Ranges for themal and ICRF contributions (2-strap or 3-strap with 1 MW) are illustrated by rectangles. (For interpretation of the references to colour in this figure legend, the reader is referred to the web version of this article.)

The estimates of the W sputtering rate, presented in Fig. 8 for P_{ICRF}=10 MW, are also made conservatively, using the affected area formed by the full antenna circumference and an additional safety margin of factor of 2, accounting for RF sheath effects along the field lines etc. The parallel W flux is integrated over the radial decay of the density, using the highest possible e-folding length available from the predicted profiles. Three reference densities shown by the vertical grey lines in Fig. 8: lowest density from 2010, as well as the highest operational densities from 2010 and from 2023.

For the more practical poloidal phasing (0; −π/2) for one antenna, toroidal (0; π; π; 0) is the most convenient option at lowest density, as it maximizes the coupling. At high densities, the toroidal phasing can be switched to (0; π; 0; π) "tapered" optimized in terms of the near-fields and reduced sputtering. This possible course of action is shown in Fig. 8 by the dotted lines with arrows and would allow to keep the ICRF-specific W rate at 10 MW below 6 % of the total W rate, as well as below 16 % of the W rate at the outboard wall at the highest possible density. The total W rate of $5.5 \cdot 10^{20}$ s^{-1} and the W rate at the outboard wall of $2 \cdot 10^{20}$ s^{-1}, shown in Fig. 8 as horizontal grey dashed lines, were estimated separately using a sophisticated approach without ICRF effects [21] and were provided by the IO. At P_{ICRF}=20 MW, the maximum relative contributions of the ICRF-specific W sources are 10 % to the total and 25 % to the outboard wall W sources respectively.

In contrast to many experiments, the outer wall area affected by the ICRF sheaths in ITER will be significantly lower compared to the area of the outer wall exposed to the thermal sheaths. Hence the relative role of the ICRF-specific W source is a-priori limited, when the W sputtering is substantial already with the thermal sheaths. This is demonstrated in Fig. 9 which shows the fraction of the ICRF-specific W rate w.r.t. the outboard wall contribution to the W sources without ICRF. The latter is

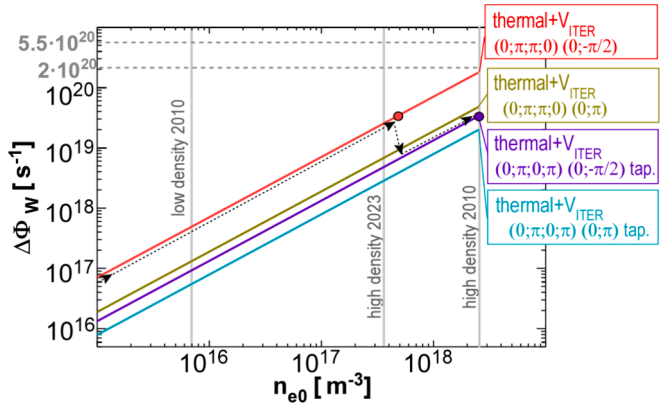

Fig. 8. ICRF-specific W sputtering rate for P_{ICRF}=10 MW as a function of n_{e0}.

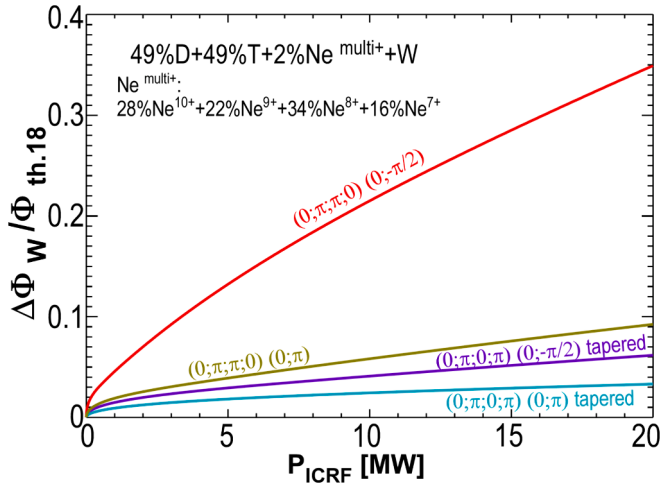

Fig. 9. ICRF-specific W sputtering rate relative to the thermal contribution of 18 equivalent ports, as a function of ICRF power.

assumed here to be a sum of 18 equivalent outer midplane ports with the same surface area as for the ICRF case, but only with the thermal sheaths. This estimated thermal contribution from the outboard wall is close to $8{\cdot}10^{20}$ s^{-1}, exceeding the provided W source estimate mentioned above by 4 times. Thus, the model used in this work generally overestimates W sources, and the relative ICRF-specific W source with the optimized (0; π; 0; π)(0; −π/2) feeding is actually limited by 6 % at P_{ICRF}=20 MW.

5. Conclusions

AUG He experiments demonstrate the importance of a precise phasing control of the W-coated 3-stap antennas which allows a reduction of the ICRF-specific W content in He plasmas to the level about twice lower than that for the B-coated 2-strap antennas, presumably by reducing both local and remote W sources.

Studies of the ITER-like low-density SOL in AUG D plasmas, by extending the region of the propagating SW in front of the PFCs, shows that the near-fields and the W sputtering characteristics are similar to those in the higher density SOL, when the SW propagation region is narrow in the limiter shadow. This allows the use of the existing guidelines to reduce the sputtering, elaborated at high SOL density.

The ITER ICRF antenna design with 4 toroidal strap columns compares favourably with the experimentally tested 3-strap antenna in ASDEX Upgrade. The ITER ICRF system allows the optimization of the electrical settings and minimizes the near-fields. The ICRF-specific increment of the W sputtering rate during ICRF operation at up to 20 MW for the D-T case with Ne seeding can be kept below 10 % of the total W wall rate without ICRF and below 25 % of the W rate at the outer wall without ICRF.

CRediT authorship contribution statement

V. Bobkov: Writing – review & editing, Writing – original draft, Visualization, Validation, Software, Project administration, Methodology, Investigation, Formal analysis, Conceptualization. **R. Bilato:** Writing – review & editing, Resources, Methodology, Investigation, Conceptualization. **F. Calarco:** Supervision, Resources, Methodology, Conceptualization. **L. Colas:** Writing – review & editing, Validation, Investigation. **R. Dux:** Resources, Methodology, Data curation. **G. Grenfell:** Software, Resources, Methodology, Data curation. **W. Helou:** Writing – review & editing, Supervision, Resources, Project administration, Methodology, Investigation, Conceptualization. **D. Milanesio:** Software, Resources, Methodology, Data curation. **R. Ochoukov:** Writing – review & editing, Methodology, Investigation, Formal analysis. **F. Paulus:** Resources, Methodology, Data curation. **Th. Pütterich:** Resources, Methodology, Data curation. **G. Urbanczyk:** Resources, Methodology, Investigation, Data curation, Conceptualization. **M. Usoltseva:** Resources, Methodology.

Declaration of competing interest

The authors declare the following financial interests/personal relationships which may be considered as potential competing interests: Part of this work has been conducted under contract IO/20/CT/4300002150. The views and opinions expressed herein do not necessarily reflect those of the ITER Organization.

Data availability

The authors do not have permission to share data.

Acknowledgement

Part of this work has been conducted under contract IO/20/CT/4300002150. The views and opinions expressed herein do not necessarily reflect those of the ITER Organization. Parts of this work have been carried out within the framework of the EUROfusion Consortium, funded by the European Union via the Euratom Research and Training Programme (Grant Agreement No 101052200 — EUROfusion). Views and opinions expressed are however those of the author(s) only and do not necessarily reflect those of the European Union or the European Commission. Neither the European Union nor the European Commission can be held responsible for them.

References

[1] V. Bobkov, et al., Impact of ICRF on the scrape-off layer and on plasma wall interactions: From present experiments to fusion reactor, Nucl. Mater. Energy 18 (2019) 131–140, https://doi.org/10.1016/j.nme.2018.11.017.
[2] P. Barabaschi, et al., Progress on ITER manufacturing, construction, commissioning and plans, IAEA 29th FEC, Oct 16-21, 2023, London, UK.
[3] R. Pitts et al., Plasma-wall interaction impact of the ITER re-baseline, this conference.
[4] V. Bobkov, et al., First results with 3-strap ICRF antennas in ASDEX Upgrade, Nucl. Fusion 56 (2016) 084001, https://doi.org/10.1088/0029-5515/56/8/084001.
[5] V. Bobkov, et al., Making ICRF power compatible with a high-Z wall in ASDEX Upgrade, Plasma Phys. Control. Fusion 59 (2017) 014022, https://doi.org/10.1088/0741-3335/59/1/014022.
[6] Y. Lin, et al., Physics basis for the ICRF system of the SPARC tokamak, J. Plasma Phys. 86 (2020) 865860506, https://doi.org/10.1017/S0022377820001269.
[7] A. Chomiczewska et el., ICRH-related impurity source and control across experiments in H, D, T plasmas at JET-ILW, Nucl. Fusion 64 (2024) 076058, doi: 10.1088/1741-4326/ad5369.
[8] V. Bobkov, et al., Improved operating space of the ICRF system in ASDEX upgrade, AIP Conference Proceedings 2254 (2020) 040005, https://doi.org/10.1063/5.0014238.
[9] L. Colas et al., The geometry of the ICRF-induced wave–SOLinteraction. A multi-machine experimental review in view of the ITER operation, Nucl. Fusion 62 (2022) 016014, doi: 10.1088/1741-4326/ac35f9.
[10] V. Maquet, et al., Analytical edge power loss at the lower hybrid resonance: ANTITER IV validation and application to ion cyclotron resonance heating systems, J. Plasma Phys. 87 (2021) 905870617, https://doi.org/10.1017/S0022377821001161.
[11] M.Q. Tran, et al., Status and future development of Heating and Current Drive for the EU DEMO, Fusion Eng. Des. 180 (2022) 113159, https://doi.org/10.1016/j.fusengdes.2022.113159.
[12] F. Paulus at el., ICRF resonance cones in the low-density scrape-off-layer of ASDEX Upgrade, submitted to Nucl. Fusion.
[13] D. Milanesio, et al., A multi-cavity approach for enhanced efficiency in TOPICA RF antenna code, Nucl. Fusion 49 (2009) 115019, https://doi.org/10.1088/0029-5515/49/11/115019.
[14] P. Jacquet, et al., Heat loads on JET plasma facing components from ICRF and LH wave absorption in the SOL, Nucl. Fusion 51 (2011) 103018, https://doi.org/10.1088/0029-5515/51/10/103018.
[15] W. Zhang, et al., Parametric study of midplane gas puffing to maximize ICRF power coupling in ITER, Nucl. Fusion 63 (2023) 036008, https://doi.org/10.1088/1741-4326/acb4ad.
[16] High Frequency Structure Simulator by ANSYS, http://www.ansys.com.
[17] V. Bobkov et al., Review and recommendations on the compatibility of ITER ICRF antennas with operation at full power in high-Z metallic environment, ITER_D_496LKP v3.0.
[18] L. Colas et al., Numerical assessment of ICRF-specific Plasma-Wall Interaction in the new ITER baseline using the SSWICH-SW code, this conference.
[19] G. Urbanczyk et al., Experimental and numerical assessments of ICRF-enhanced plasma-wall interaction in ASDEX Upgrade, this conference.
[20] V. Bobkov, et al., Assessment of compatibility of ICRF antenna operation with full W wall in ASDEX Upgrade, Nucl. Fusion 50 (2010) 035004, https://doi.org/10.1088/0029-5515/50/3/035004.
[21] K. Schmid, Full W ITER: assessment of expected W erosion and implications of boronization on fuel retention, *this conference*.